Izv. VUZ «AND», vol.10, № 3, 2002

NONLINEAR DYNAMICS OF SPATIAL AND TEMPORAL PATTERNS IN LASERS AND ATOM OPTICS: KERR-LENS MODE-LOCKED LASER, ZEEMAN LASER AND BOSE-EINSTEIN ATOMIC CONDENSATE

L.A. Melnikov, A.I. Konukhov, I.V. Veshneva, V.L. Derbov, V.V. Serov

Nonlinear dynamics of spatial and temporal behaviour of laser and atom optical systems is investigated numerically. Systems with nearly one scalar transverse mode (Kerr-lens mode-locked laser), with large number of vectorial transverse modes (Zeeman laser with large Fresnel number and anisotropic cavity), and non-ground collective states of Bose-Einstein condensate of trapped neutral atoms are considered. Attempts to classify the complex transverse polarization pattern dynamics are made basing on the vectorial Karhunen-Loeve modes and their singularity points character, including catastrophes and Newton diagrams. Excitation of non-ground states of atomic Bose-Einstein condensate via resonant perturbation is analyzed.

Introduction

Nonlinear dynamics in lasers and optical systems is at present mainly addressed to the models which incorporate the distributed nature of these systems. Since the nonlinearity in lasers is not large, the laser field can be treated as a superposition of longitudinal and transverse empty-cavity modes coupled via linear and nonlinear elements in the cavity. Huge number of different regimes can be realized in lasers, depending on the active medium and cavity parameters. However, two different limit cases are of primary interest: (i) huge number of longitudinal modes and small number of transverse modes, and (ii) small number of longitudinal modes and large number of transverse modes. If all modes oscillate with definite phases, the laser output appears to be a regular sequence of ultra-short pulses for case (i) and a regular motion of light intensity spots in the transverse plane for case (ii). These regimes are often referred as mode-locked regimes, and the investigation of their stability and destruction is a challenging problem, taking the practical importance of these regimes into account. It is well known that mode locking is the only way to produce extremely short (a few femtoseconds) laser pulses.

On the other hand, there exist systems described by equations, similar to those of nonlinear paraxial optics, but with nonlinearity huge compared with that of optical systems. An important example of such a system is the Bose-Einstein condensate (BEC) of neutral trapped atoms whose wave function in the mean-field limit obeys the Schrödinger-type equation with large qubic nonlinear term proportional to the number of

atoms. Investigations of the dynamics of BEC are of interest in the context of its promising applications in atom optics.

The study of the dynamics of these distributed systems in essentially nonlinear regimes is possible if we have (i) powerful methods for numerical modeling of the underlying physical processes, and (ii) means and approaches for the description of the resulting dynamics of distributed systems. The last condition is vital for the description of multitranverse polarization pattern dynamics. In this paper we present the models and numerical results related to the dynamics of the above-mentioned systems, the possible way for the classification of the regimes and excitation of nonlinear stationary states.

As an example of a laser system with large number of longitudinal modes we consider the Kerr-lens mode-locked laser. The full spatial-temporal model of this laser is presented and used for numerical investigations of the nonlinear dynamics of *Z*-cavity Ti:Sph laser with Kerr-lens mode locking (KLM).

In the mode-locked regime the laser output represents a pulse train with the repetition rate determined by the cavity round trip time $2L/c$, where L is the cavity length. Kerr nonlinearity of intracavity elements provide intensity-dependent phase shift, thus inducing a lens-like medium with the intensity-dependent focal power. In specially designed cavities a spatially narrow gain profile or a physical aperture can provide intracavity losses which decrease almost instantaneously with the intensity. This makes the Kerr-lens mode locking to be a powerful technique for generating femtosecond pulses.

In time domain the Kerr nonlinearity in combination with the negative group velocity dispersion (GVD) leads to the solitonic pulse shaping [1, 2]. The pulse amplitude modulation due to Kerr-lens effect is usually treated as the effect of fast saturable absorber [5, 6]. For the mode locking process to be self-starting, the power-dependent losses must exceed a definite value [1, 7]. The optimum resonator parameters are derived with the help of the nonlinear ABCD-matrix formalism [5, 8, 9, 10, 11, 15].

The Schrödinger equation for the field envelope was completed with gain, losses, high-order dispersion terms [16, 17], Bloch equations for the coherent semiconductor absorber [18], stimulated Raman gain [19] and then either solved numerically or evaluated analytically using the hyperbolic secant ansatz for the solution [14, 3, 4]. This allows one to estimate the pulse chirp, pulse width and stability conditions. The pulse energy increase or the reduction of the negative group delay dispersion can result in the pulse instability [3], as well as the finite bandwidth of the gain and the reflecting mirrors [4] or the gain depletion and recovery during the pulse round-trip [20].

For certain conditions KLM lasers demonstrate instability of the pulse train [21, 22]. Quasi-periodic and chaotic oscillation regimes [26], bifurcation of the fundamental mode [27] arise due to the nonlinear coupling of geometrical and energetic characteristics of the beam due to Kerr effect. KLM lasers can keep a small portion of lasing energy in higher-order transverse modes [25]. The dynamical instabilities can be associated with the transverse mode beating [23, 24, 28].

The time-domain ABCD-law [29] in conjunction with ABCD-law for a Gaussian beam allows one to construct an iterative mapping for the beam and pulse parameters [30, 31, 32]. Numerical simulation reveals the evidence of quasi-periodical and chaotic behaviour of both the beam and the pulse parameters [30, 33].

In this paper we present a model with no limitations of pulse and beam shape. The transverse and temporal evolution of a pulsed beam is governed by the paraxial wave equation, which is solved in terms of Laguerre-Gauss modes. For simplicity we consider axially symmetric beams. A prominent feature of our model is that we take into consideration the temporal evolution of the active medium polarization (i.e., the gain and dispersion) during the pulse. The spatio-temporal profile of the gain is directly calculated from the density matrix equations for two-level media. Simultaneous treatment of spatial

and temporal field distribution inside the cavity enables one to consider the dynamics and the transient processes during the build-up of the oscillation regime. Our model is not restricted to small round-trip changes of the transverse beam profile, round-trip gain, dispersion and amplitude modulation coefficient. It takes into account the amplitude modulation of the pulse due to self-focusing, the nonlinear mode coupling via the medium polarization, and the gain aperturing.

As an example of a laser system with large number of transverse mode we consider the Zeeman laser with anisotropic cavity [49]. Correct description of the polarization transverse pattern dynamics in lasers with large number of transverse modes is a challenging problem for laser dynamics [35, 28, 36, 37, 38]. For the classification of the structures of the laser field its singular points (zeroes, saddle points, maxima and minima) can be used [39, 40]. However, in these papers the models of the laser fields are far from reality. Another approach utilizing the hierarchy of symmetry breaking was also used for the classification of the regimes [41, 42].

An efficient approach to the analysis of very complicated signals and processes is based on Karhunen-Loeve procedure [44, 45, 46, 43, 47, 48, 49]. In [49] the laser regimes with rotating patterns were investigated and it was shown that these regimes are connected with catastrophes A_n of $x \pm iy$ arguments, where x, y are the transverse coordinates. In the present work we also used Karhunen-Loeve modes (KL-modes), however, we added the laser regimes corresponding to oscillating patterns. We introduce the vector Karhunen-Loeve modes, transform the four-dimensional vector field, representing the polarized laser transverse patterns, to the two-dimensional vector field, representing the transverse distribution of the Stokes parameters (2DSP), discuss some properties of this 2D vector field and try to classify the structures in accordance with the behaviour of the 2D vector field near the singularity points. For the oscillating patterns 2DSP does not belong to the gradient case [49]. We propose to use Newton diagram method for the investigation of singular points of the 2DSP vector field.

Bose-Einstein condensates of neutral trapped atoms have become a subject of numerous and extensive studies (see, e.g., the reviews [54, 55, 56]) as a new state of matter with properties opening new possibilities in atomic optics and related fields. One of the most exciting features is the possibility to construct atom lasers. In the present paper we report some new dynamical properties of the Bose-Einstein condensate of atoms in a harmonic trap. In contrast to the optical systems, the nonlinear terms in the equation governing the collective wave function, are typically dominating and, generally, cannot be treated as a perturbation, thus making the eigenfunction problem to be essentially nonlinear. In the present paper the non-ground stationary states of BEC are calculated, and the dynamics of these states under resonant perturbation of the trapping potential is investigated.

2. Kerr-lens mode-locked laser

2.1. Theoretical model. The model was developed assuming the amplitude of the electric field F to be varying slowly. For numerical simulations the Z-cavity configuration was taken (Fig. 1, *a*). To calculate the electric field envelope dynamics we consider the field passing the optical elements of the cavity from the plane of aperture A_1 to the plane of aperture A_2 and then returning back. For simplicity we consider the stigmatic case. Schematic equivalent diagram of the Z-cavity is shown in Fig. 1, *b*. The spherical mirrors of the folded cavity are replaced by lenses of the same focal power $F=2/R$, where R is the curvature radius of the mirror. The round-trip change of the electric field envelope was obtained by applying transfer operators in the order of their action in the cavity.

Assuming the cylindrical symmetry of the cavity, the expression for the field at any

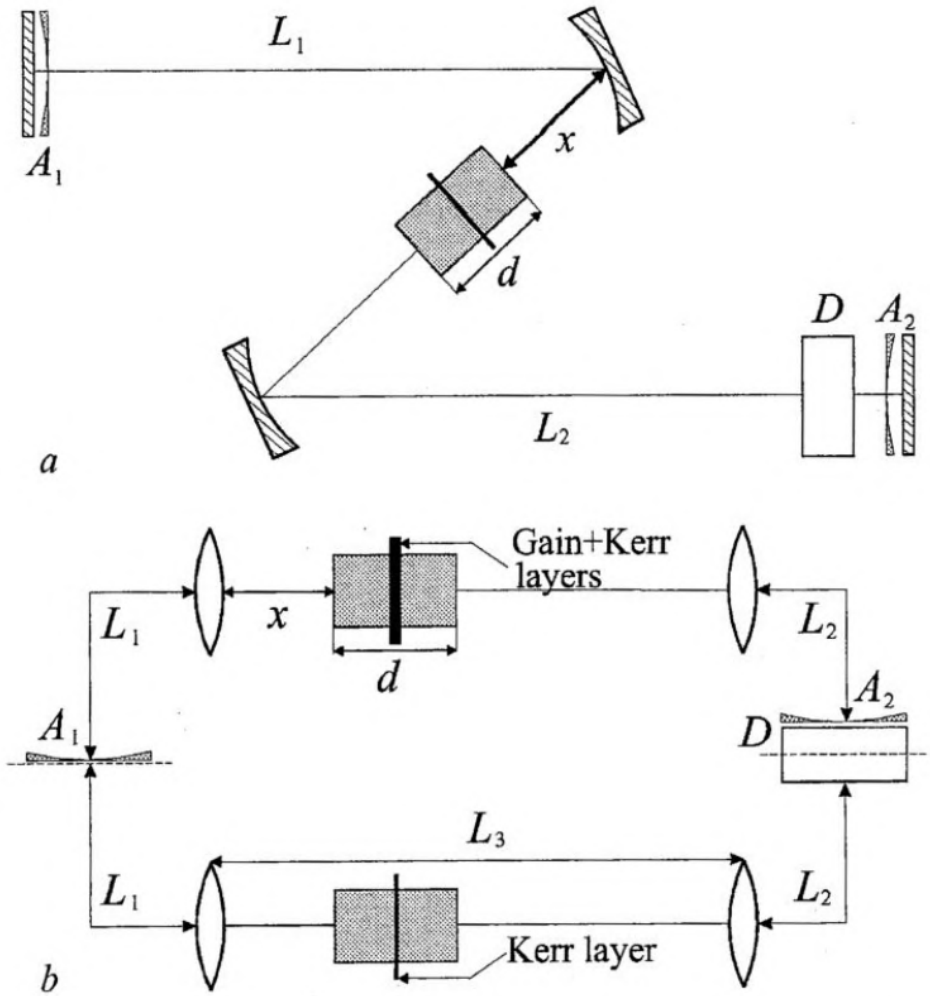

Fig. 1. Cavity configuration (*a*) and its equivalent diagram (*b*). A_1, A_2 are the Gaussian apertures near the plane mirrors. L_1, L_2, L_3 are the arm lengths of the cavity. d is the rod length, x is the distance between the mirror and the rod, D denotes the dispersion element

transverse plane $z=z_0$=const may be written in terms of Laguerre-Gaussian mode amplitudes:

$$E(z_0,r,\tau) = \Sigma_j\ A_j(z_0,\tau)\, L_j(\eta(z_0)r^2)\, \exp(-P(z_0)r^2/2), \qquad (1)$$

where j is the mode index, L_j are the Laguerre polynomials, r is the transverse radius, $\tau=t-z/c$ is the local time in the running coordinate system z, $\tau-z/c$, $P(z)=\eta(z)+i\xi(z)$ is the complex beam parameter of the empty cavity, normalized to the value of k/l, where $k=2\pi/\lambda$ is the wavenumber, λ=800 nm is the wavelength of the fluorescence peak, l=1 mm is the unit length of the propagation distance.

The mode amplitudes $A_j(0,\tau)$ at the initial plane $z=z_0$ are defined by the integral transformation

$$A_j(z_0,\tau) = 1/(2\eta)\int_0^\infty rdr\, E(z_0,r,\tau)\, L_j(\eta(z_0)r^2 \exp(-P^*(z_0)r^2/2), \qquad (2)$$

while the modal amplitudes and the beam parameters at arbitrary point z during the free-space propagation are given by

$$A_j(z,\tau) = A_j(0,\tau)\,[1 + i(z/n)\,P(0)]^{-1}\exp(i\,\varphi_j),$$

$$P(z) = P(0)\,[1 + i\,(z/n)\,P(0)]^{-1}, \qquad (3)$$

$$\varphi_j = -2j \arg\,(1 + i\,(z/n)\,P(0)),$$

where $P(0)$ is the beam parameter at the initial plane $z=0$, n is the refractive index.

The transformation of the beam parameter and mode amplitudes at the mirrors (lenses) is

$$P(2) = P(1) + iF, \quad A_j(2,\tau) = A_j(1,\tau)\,T^{1/2}, \qquad (4)$$

where 1, 2 denote the input and output planes of the mirror, $F=2/R$ is the mirror optical power, T is the uniform power transmission coefficient.

The masking of the beam by the aperture with Gaussian transmission profile was taken into account in a way similar to [28]. For the transmission function of the aperture $T_a(r^2)=\exp(-\eta_a r^2/2)$

$$P(2) = P(1) + \eta_a,$$

$$A_j(2,\tau) = \Sigma_k\, A_k(1,\tau)\, L_{jk},$$

$$L_{jk} = \int_0^\infty L_j(x')\,L_k(x)\exp(-x')\,dx' = \begin{cases} (-1)^k\,(j+k)!\;\sigma^{k-j}/(j\,!(-j-k)_k\,(1+\sigma)^k), & j \le k \\ 0, & j > k, \end{cases}$$

where $x=\eta r^2$, $x'=(\eta+\eta_a)r^2$, η is the real part of the beam parameter P before the aperture, $\sigma=\eta_a/\eta$.

The transformation of the beam parameter per one round-trip obeys the well-known ABCD-law:

$$P(z+L) = P(z), \quad P(z+L) = (A(z)P(z) + B(z)) / (C(z)P(z) + D(z)),$$

where $\begin{pmatrix} A & B \\ C & D \end{pmatrix}$ is the matrix of the cavity round-trip. This matrix is a product of the matrices

$$\begin{pmatrix} 1 & 0 \\ izn^{-1} & 1 \end{pmatrix}$$

for propagation through a homogeneous medium of the length z and refractive index n,

$$\begin{pmatrix} 1 & iF \\ 0 & 1 \end{pmatrix} \qquad (5)$$

for a mirror with optical power F,

$$\begin{pmatrix} 1 & \eta_a \\ 0 & 1 \end{pmatrix}$$

for an aperture.

The thin dispersion element was placed near A_2 aperture of the right arm of the cavity (see Fig. 1). Assuming the effect of diffraction to be small, the equation for the mode amplitudes can be written as follows

$$\partial A_j(z,\tau)/\partial z = -i\,(\kappa_2/2)\,(\partial^2 A_j/\partial\tau^2).$$

For the chosen amplitude of electric field E negative κ_2 corresponds to the negative group velocity dispersion. To calculate the modal amplitudes after the dispersion elements the Fourier transform method was used. It allows one to add linear dispersion terms of higher order and nonlinear group velocity dispersion [2].

For our calculations 15 Laguerre-Gaussian modes were used. After several thousands of the cavity round-trips the transient evolution was finished and the spatial and temporal dependencies were saved and analyzed.

To find the pulse transformation after the laser crystal the split-step method is used. The rod is divided in two parts (Fig. 1). We assume the active medium to be thin. The thin active layer is placed in the middle of the medium having the refractive index n. In the space of half rod length $d/2$ the mode amplitudes are calculated using (3). In the plane of the active layer the radial grid (r_i) is chosen. In each of the grid points the field $E(r_i,\tau)$ is calculated using (1), then the field equation is solved:

$$\partial E(z,r,\tau)/\partial z = -(G/2)iP(z,r,\tau) + i\,\beta|E|^2E. \qquad (6)$$

Here G is the non-saturated power gain, β is the Kerr constant, $P(z,r,\tau)$ is the medium polarization given by the density matrix equations (Bloch equations). In the thin layer the diffraction and dispersion are not taken into account.

We use the full set of Bloch equations for a two-level medium to simulate the oscillation regimes when the pulse width and the relaxation time of the medium polarization are of the same order.

$$\partial P/\partial\tau = -(\Gamma + i\,\Delta)P + iE(N_u - N_l)\Gamma, \qquad (7)$$

$$\partial N_l(z,r,\tau)/\partial\tau = -\gamma_l N_l + \mathrm{Im}(E^*P)\gamma_l\gamma_u/(\gamma_l+\gamma_u), \qquad (8)$$

$$\partial N_u(z,r,\tau)/\partial\tau = -\gamma_u(N_u - N_u^0) - \mathrm{Im}(E^*P)\gamma_l\gamma_u/(\gamma_l+\gamma_u), \qquad (9)$$

where Γ, γ_l, γ_u, are the relaxation rates of the medium polarization and the populations of upper (u) and (l) lower levels, respectively, $N_l(z,r,\tau)$, $N_u(z,r,\tau)$ are the populations normalized to the unsaturated value of N_u, $\Delta=\omega_0-\nu_0$ is the frequency detuning, ω_0 is the transition frequency. The field $E(z,r,\tau)$ is normalized so that $|E|^2$ is the dimensionless intensity. At each of the transverse grid points r_i for given $E(r_i,\tau)$ the value of $P(r_i,\tau)$ is calculated using the second-order Adams scheme. In order to simulate the spontaneous emission effect the random short pulses are added to the field amplitude at each of the grid points. The effect of soft aperturing on the active medium is approximated by a Gaussian aperture placed near the thin active layer.

2.2. The cavity parameters. For the empty cavity we chose the total power transmittance of the aperture to be A_1~75% (Fig. 1). The transmittance of the aperture A_2 did not exceed 99.5%, having no effect on the pulse formation. The coefficient in (4) was taken to be T=0.95. The focal power of the lenses was $F=2/R$, R=100 mm. We have performed the numerical calculations for the symmetric cavity with $L_1=L_2$=850 mm. The rod length was d=20 mm, the refractive index of the rod of Ti:Sph was n=1.76, the cavity detuning Δ=0 (7), the relaxation rate of the medium polarization Γ=0.31 fs^{-1}, the relaxation rates for the upper and lower levels $\gamma_l=2\cdot10^{-4}$ fs^{-1}, $\gamma_u=2\cdot10^{-9}$ fs^{-1}, the dimensionless Kerr constant $\beta=(k/l)nn_2I_s$, where $n_2=3.2\cdot10^{-16}$ cm^{2}W^{-1} [1], the saturation intensity I_s=290 kW/cm^2 [13].

The optimal configuration for mode locking gives the nonlinear loss coefficient [5, 6] $\delta=dL/dW$, where L presents the differential cavity losses for the distributed laser model. For the discrete-element laser model the power dumping satisfies the round-trip equation $W^{(2)}=\Theta W^{(1)}$, where $W^{(1)}$ is the power before the cavity round trip and $W^{(2)}$ is the power after one round trip. Correspondingly,

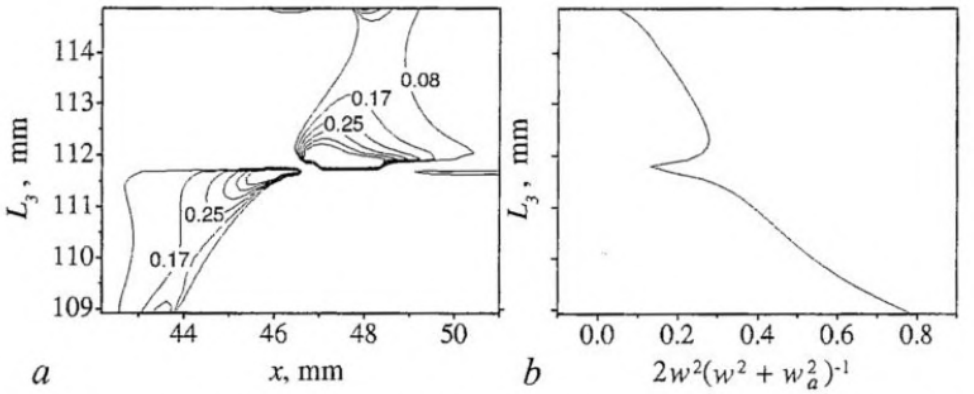

Fig. 2. Contour lines of the $w^{-1}(dw/dW)$ coefficient as a function of the rod position x and of the folding distance L_3 (a). Only positive values are shown. Data labels are in $10^{-6}W^{-1}$ units. Coefficient $2w^2(w^2+w_a^2)^{-1}$ (11) for aperture A_1 (b). The dimensionless aperture width $w_a^2=2\eta_a^{-1}$ is fixed at the value $0.37\cdot10^4$

$$L = -\ln\Theta, \qquad \delta = -(1/\Theta)(d\Theta/dW)_{|W=0}. \tag{10}$$

For one intracavity aperture

$$\Theta = T\eta(\eta+\eta_a)^{-1}, \qquad \delta = -(2w^2/(w^2+w_a^2))\,(1/w)\,(dw/dW)_{|W=0}, \tag{11}$$

where $\eta=2w^{-2}$ is the real part of the beam parameter before the aperture, $\eta_d=2w_d^{-2}$ is the aperture parameter.

To calculate the value of δ the ABCD-matrix formalism was used. The thin Kerr layer was approximated by the lens (5) with the focal power $F=2\mathrm{Re}(P)^2\beta dW/\pi$, where P is the stationary beam parameter in the middle of the laser rod, dW is the power deviation from the zero value.

For L_3=111.8 the cavity is equivalent to the confocal one [6]. The upper half plane L_3>111.8 (Fig. 2, *a*) contains a wider region for stable mode locking. In the experiments [6, 12] this is referred as a region of low sensitivity to the misalignment of the mirrors and the laser rod.

2.3. Numerical results and discussion. To characterize the output pulsed beam we expressed the intracavity power in Watts, while the pulse energy and the beam cross-section area were scaled to their stationary values. The field was calculated in the fixed time frame. We calculated also the pulse shift s from the frame center and the pulse width τ_0. For the chosen aperture transmission and uniform loss the differential losses are 0.35. For G above this value we have obtained the mode-locking regime (Fig. 3).

As seen from Fig. 3, *a*, at the pulse peak the beam has the smallest transverse dimension. In addition to the solitonic pulse shaping this effect leads to the pulse shortening. In spite of the perfect pulse symmetry (Fig. 3, *b*) the relative beam area $\sigma(\tau)$ has an asymmetry with the respect to pulse peak. This asymmetry arises due to effect of finite relaxation time of the gain media. For longer pulses, which can be obtained for the same cavity configuration by increasing of the GVD-magnitude, such asymmetry is absent.

The relation between the solitonic pulse shaping and the pulse compression due to Kerr-lens effect is given by the factor [1]

$$R = (1/2\pi)(\beta J/|D|). \tag{12}$$

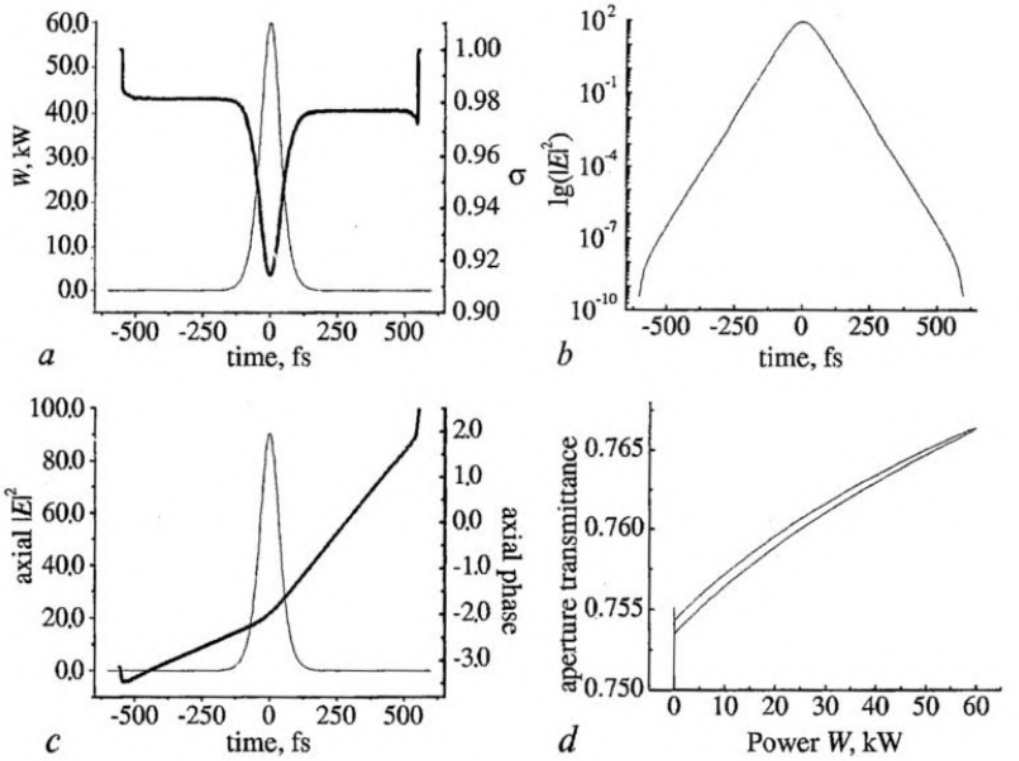

Fig. 3. Pulsed beam characteristics before the aperture A_1. The folding distance L_3=112 mm, the rod position x=47 mm. The round-trip power gain G=0.38. Power and relative beam area versus local time (*a*). Decimal logarithm of the axial intensity versus time (*b*). Axial intensity $|E|^2_{r=0}$ and axial phase $\arg(|E|^2)_{r=0}$ versus time (*c*). Aperture transmittance $w_a^2(w(\tau)^2+w_a^2)^{-1}$ versus beam power (*d*)

For the regime shown in Fig. 3 J=5 nJ which yields R=0.25. Therefore, the solitonic pulse shaping is predominate. Logarithmic plot versus the axial intensity reveals the pulse shape closer to sech $(\tau/\tau_0')^2$ (Fig. 3, *b*). The phase of the field shows the presence of pulse chirp. The linear part of the chirp corresponds to the pulse retardation with respect to the pulse propagation without the active medium. In other words, the pulse repetition rate is less than the reciprocal round trip time.

Estimating the power-dependent losses δ by means of the ABCD-matrix formalism for L_3=112 mm, x=47 mm we have found $\delta=0.43\cdot10^{-6}$ W^{-1}. To compare this value with the result of numerical simulations of mode-locking regime we have calculated the beam transmittance of the aperture A_1 (Fig. 3, *d*). Calculating the nonlinear loss coefficient (10) at $W\sim0$ we get $\delta=0.4\cdot10^{-6}$ W^{-1}, which is in agreement with our assumption. For higher power the weak saturation arises decreasing the magnitude of δ. Indeed, the effect of finite relaxation time causes a slight asymmetry in the transmission of the pulse front and the pulse train (Fig. 3, *d*).

The aperture transmittance can be calculated: i) by direct calculation of power before the aperture and after it; ii) as $w_a^2(w(\tau)^2+w_a^2)^{-1}$ in assumption of Gaussian intensity profile having the width $w(\tau)^2=\sigma(\tau)w_0^2$. Both methods give the same results, due to perfect approximation of the output beam by Gaussian. Besides, the analysis of spatio-temporal beam profile shows that the pulse width is independent of the radial coordinate.

The gain increase leads to the increase of the power dependent loss $W\delta$. As a consequence, the pulse width is decreased (Fig. 4, *a*).

We have calculated also the pulse shift s. The minimal pulse shift corresponds to

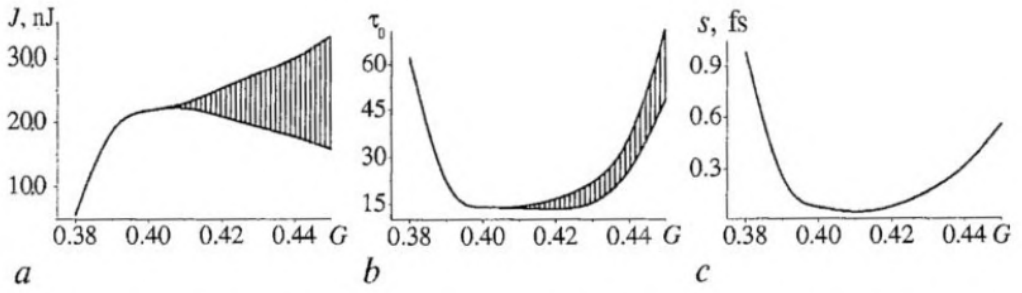

Fig. 4. Pulse width (*a*), averaged pulse shift per round trip (*b*) and pulse energy (*c*) versus round-trip power gain. The filled area shows the boundaries for the pulse energy (*a*) and pulse width (*b*) in the regime of pulse-train periodic instability

the maximal repetition rate, that corresponds to the minimum of the pulse width (Figs 4, *b, c*). This tendency is common for mode locking regimes. For example, at the rod position x=47 mm and the folded mirror distance L_3=112.5 mm the magnitude of the nonlinear loss coefficient δ is not sufficient to develop a pulse train instability up to $G<0.6$.

Before achieving the minimal width (Figs 4, *a*, 5, *a*) the pulse can be well approximated by the hyperbolic curve $\tau_0(J)=\pi/6^{1/2}\kappa_2(\beta J)^{-1}$ [1] as a function of the pulse energy. For higher gain values the parameter $R\geq 1$ (12), which corresponds to the breakdown of the weak-pulse-shaping approximation in the description of femtosecond pulses.

For given cavity configuration the phase delay per round-trip for each Laguerre-Gaussian mode of the empty cavity is close but not equal to 2π. That is possible only for the unstable cavity configuration. Due to the mismatch between the phases of transverse modes quasiperiodic regimes are possible. Up to a definite value of gain the nonlinear medium gives rise to the locking of phases of mode amplitudes. Larger nonlinearity initiates distortion of the mode-locked regime. Earlier works [23, 24] have shown that very small amplitudes of higher-order transverse modes can give rise to quasiperiodic oscillation. Additional pulse instability arises due to the propagation of nonlinearly chirped pulse in the dispersive medium [1].

Pulse train periodic instability occurs starting with round-trip gain value $G>0.41$ (Fig.4, *a, b*). At the instability threshold we observed significant temporal variations of the spatial beam size (Fig. 6, *a*)

Logarithmic plot versus the axial intensity reveals the wing structure of the pulse (Fig. 6, *b*). The pulse shape significantly differs from sech^2. Moreover, the variation of the temporal profile from one transverse point to another was observed.

Due to the variation of the spatial beam size (Fig. 6, *a*) the pulse chirp has a

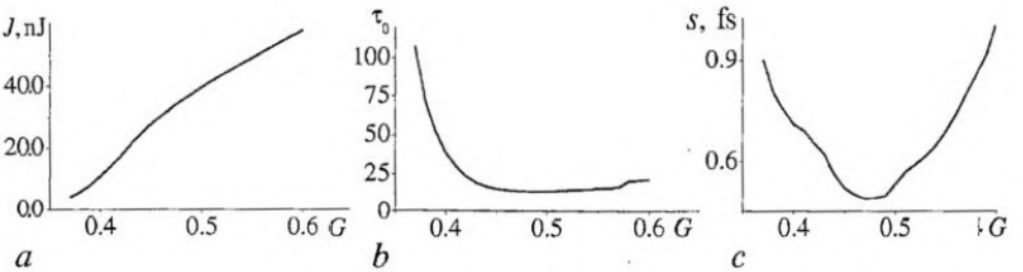

Fig. 5. x=47 mm, L_3=112.5 mm. Pulse width (*a*), averaged pulse shift per round trip (*b*), and pulse energy (*c*) versus round trip gain

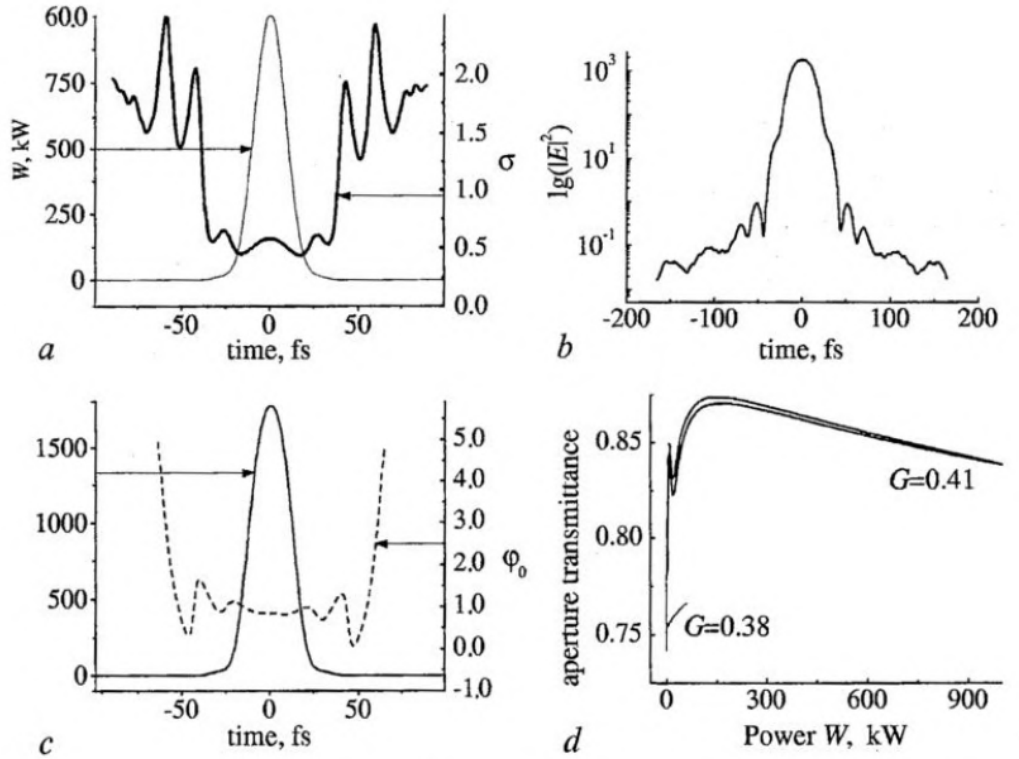

Fig. 6. Pulsed beam characteristics before the aperture A_1. The folded mirror distance and the rod position are unchanged. The round-trip power gain is G=0.41. Power and relative beam area versus local time (*a*). Logarithm of base 10 from axial intensity versus time (*b*). Axial intensity $|E|^2_{r=0}$ and axial phase $\arg(|E|^2)_{r=0}$ versus time (*c*). Aperture transmittance $w_a^2 (w(\tau)^2+w_a^2)^{-1}$ versus beam power (*d*)

significant nonlinear part. However, for this regime the pulse shift has a minimum (Fig. 4, *c*).

Fig. 6, *d* shows the fractional power transmitted by the aperture A_1. For comparison two curves are shown: near the gain threshold (G=0.38) and close to the start of the pulse-train periodic instability (G=0.41).

The oscillation regime for G=0.43 is shown in Fig. 7. The curve showing the dynamics of pulse width (Fig. 7, *a*) has small spikes in front of one period of oscillations, but the pulse energy smoothly varies from one round trip to another.

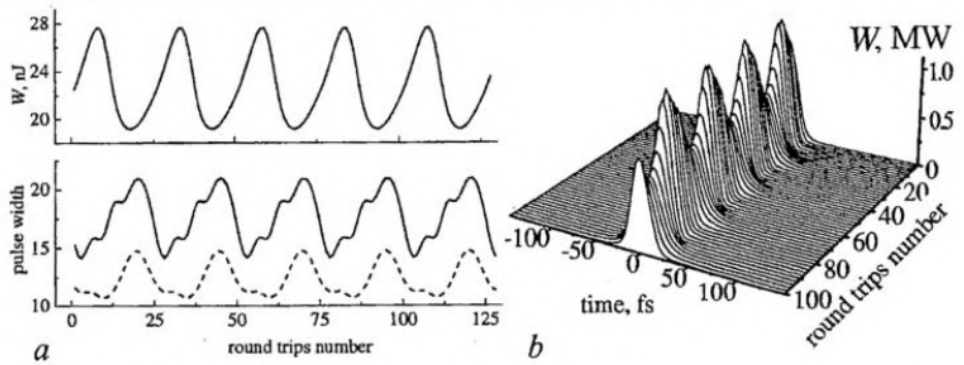

Fig. 7. G=0.43. Other parameters are unchanged. Pulse energy and pulse width versus round trips number (*a*). The pulse width shown by the solid curve was calculated as the second moment, the dashed curve corresponds to the pulse width defined at the sech(1)^2 level. Temporal dynamics of the beam power (*b*)

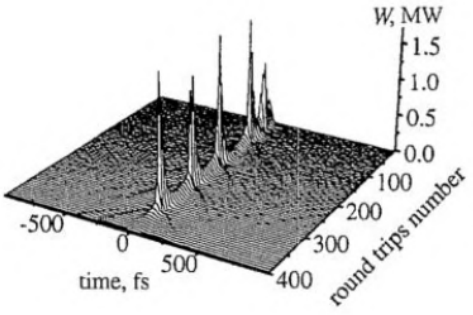

Fig. 8. Temporal dynamics of the beam power for G=0.46

At larger gain the magnitude of oscillations is growing (Fig. 8) which breaks the pulse train.

The growth of the oscillation magnitude is accompanied by successive excitation of several equidistant frequencies in the Fourier spectrum of the pulse energy evolution. The ground oscillation frequency depends on the GVD, the rod position and folded mirror distance.

3. Transverse pattern dynamics in Zeeman laser

3.1. Karhunen-Loeve vectorial modes. The electric field vector in the transverse plane of a laser can be expressed in the paraxial approximation as follows:

$$\mathbf{E}(x,y,z,t) = \Sigma_{q=-1,1} (-1)^q E_q(t)\, \mathbf{e}_{-q}.$$

The spherical component of the field E_q can be expressed in terms of the amplitudes of right and left polarized waves A_q

$$E_q = A_q (r, \varphi, z, t) \exp(i\nu t - iKz) + A_{-q}^*(r, \varphi, z, t) \exp(-i\nu t + iKz),$$

where (r,φ) are the polar coordinates, q=±1.

To describe the complex spatio-temporal laser dynamics we use the Karhunen-Loeve procedure in which it is necessary to calculate the eigenvectors and eigenvalues of the normalized correlation matrix 2×2, obtained by time averaging of the product of normalized field components at two different points in the transverse plane. It is often more convenient to work with a matrix equation rather then with an integral equation. This can be done using the field decomposition in terms of Laguerre-Gaussian (LG) modes. For a fixed transverse plane z=const in the laser cavity

$$A_q(r,\varphi,t) = \Sigma_{m=-\infty}^{\infty} \Sigma_{n=0}^{\infty} A_n^m(t)_q \psi_n^m(r,\varphi), \tag{13}$$

where $A_n^m(t)_q$ is the mode amplitude,

$$\psi_n^m(r,\varphi) = L_n^{|m|}(\eta(z)r^2)\, (\eta r^2)^{|m|/2} \exp(-P(z)r^2/2 + im\varphi),$$

$$\langle \psi_n^m \mid \psi_{n'}^{m'*} \rangle = N_n^m \delta_{mm'} \delta_{nn'}.$$

Here P is the complex beam parameter at the chosen z plane, L_n^m is the Laguerre polynomial, $N_n^m = 2\pi(n+m)!/n!$. It is convenient to introduce normalized mode amplitudes

$$(a_n^m)_q = (A_n^m)_q\, (N_n^m/W)^{1/2}. \tag{14}$$

In terms of Laguerre-Gaussian mode amplitudes the time-averaged total power of the beam can be written as $W=(2\eta)^{-1}\langle \Sigma_{m,n,q} N_n^m (A_n^m)_q (A_n^m)_q^* \rangle_t$.

The matrix version of the integral equation can be easily derived

$$[\Lambda, \mathbf{b}] = \lambda \mathbf{b}, \tag{15}$$

where

$$\mathbf{b} = \begin{pmatrix} (b_n^m)_+ \\ \vdots \\ (b_n^m)_- \\ \vdots \end{pmatrix}, \qquad \Lambda = \overline{\begin{pmatrix} (a_n^m)_+ (a_n^m)_+^* & \cdots & (a_n^m)_+ (a_n^m)_-^* & \cdots \\ \vdots & \ddots & \vdots & \ddots \\ (a_n^m)_- (a_n^m)_+^* & \cdots & (a_n^m)_- (a_n^m)_-^* & \cdots \\ \vdots & \ddots & \vdots & \ddots \end{pmatrix}^t}. \tag{16}$$

Here the overline denotes the time averaging.

Due to the normalization chosen (14), the matrix Λ is Hermitian and Spur(Λ)=1. Hence $\Sigma_k \lambda_k = 1$, and the eigenvectors, corresponding to the different eigenvalues, are orthogonal:

$$\mathbf{b}_k \mathbf{b}_j^* = \Sigma_{m,n,q} (b_n^m)_{q\,k} (b_n^m)_{q\,j}^* = \delta_{k,j} .$$

The laser dynamics is dominated by the modes (**b**) whose sum of eigenvalues is close to unity. Obviously, for stationary fields the KL-modes include only one mode which coincides with the field itself with the eigenvalue λ=1. In LG basis the KL-modes coincide with LG modes with amplitudes $(b_n^m)_q W/N_n^m$ and eigenvalues which are the relative intensities of modes.

3.2. Numerical model and results. We consider a Zeeman laser with nonplanar (image rotating) ring cavity with large Fresnel number [51, 49]. Fig. 9 shows the field transformation operator scheme used for numerical modeling.

For each slowly varying complex amplitude $A(r,\varphi,z,t)_q$ a paraxial wave equation similar to (6) is solved. We consider round-trip variations of the total field and describe the laser dynamics in the scale of round trip times. The field transformation during one round trip is a consequence of the following steps: i) free-space propagation; ii) image rotation; iii) Gaussian aperture and lens; iv) nonlinear active medium; v) linear cavity anisotropy.

In free-space part of the cavity we used the decomposition of each complex field amplitude in terms of Laguerre-Gauss orthogonal modes. The image rotation after one round-trip is described by the coordinate frame rotation by the angle θ, $\varphi'=\varphi-\theta$, where φ' is the azimuthal coordinate in the rotated coordinate frame

$$(A_n^m)_q' = (A_n^m)_q \exp(i\,(m - q)\theta).$$

The field transformation at the Gaussian aperture and lens was also expressed in terms of the transverse mode amplitudes [28, 51]. For simplicity a stigmatic cavity was considered. Grid representation of the field in the active medium was used. In each of the transverse polar grid points (r_i,φ_j), i=1,...,15, j=1,...,20 the field components A_q were calculated. We suppose that the active medium is thin, $\partial A_q/\partial z = iG/2P(r_i,\varphi_j)_q$, where P_q are the circular components of the medium polarization, G is the round-trip power gain.

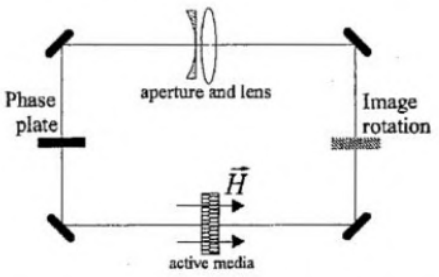

Fig. 9. Image rotating ring cavity model with axial maghetic field **H**

The active medium is supposed to have a transition j=1↔ j=2, where j denotes the angular momentum quantum number, and is placed into the homogeneous magnetic field. The density matrix equation for the irreducible spherical tensors is solved algebraically.

$$P_q = A_q D_q \frac{1+[\alpha^{(+)} - \alpha^{(-)}]S_{-q}}{1 + \alpha^{(+)}[S_q + S_{-q}] + [(\alpha^{(+)})^2 - (\alpha^{(-)})^2]S_q S_{-q}},$$

where

$$D_q = \gamma/(\gamma + i(\omega - \nu + q\Omega)), \quad S_q = |A_q|^2 \mathcal{L}_q, \quad \mathcal{L}_q = \mathrm{Re}[D_q].$$

Here γ is the relaxation rate of the medium polarization, the frequency ω is associated with the energy gap in the absence of magnetic field, Ω is the Zeeman splitting, $\alpha^{(+)}=0.46$, $\alpha^{(-)}=(0.21/\gamma_u+0.01/\gamma_l)\gamma_u\gamma_l/(\gamma_u+\gamma_l)$, where γ_u and γ_l are the relaxation rates of the upper and lower level, respectively.

Phase anisotropy of the cavity was modeled by the birefringent plate. Corresponding expression can be found in [49].

We consider a high-gain active medium and a large number of transverse modes. In numerical studies we have used more than 200 transverse modes in both circularly polarized components of the field.

In numerical experiments we used the following set of parameters: the ratio of the beam area to the area of Gaussian aperture $\eta_A=0.05$, the normalized focal power of the effective lens in the cavity $F=L/f=1.5, 2.0, 2.5$, where L is the cavity length, f is the focal distance of the lens, the Zeeman splitting normalized to the transition line width $\mu=\Omega/\gamma=0.15$, the transmission coefficients responsible for the linear amplitude anisotropy of the cavity $t_x=0.95$, $t_y=0.94$, the linear phase anisotropy (phase retardation in the birefringent plate inside the cavity) $\delta=0.1$. The round-trip gain is $G=0.52$, corresponding to the relative excitation value close to 2.0. In the regimes considered the image rotation variation affected only the power modulation frequency, leaving unchanged the transverse pattern structures. Hence we used the zero value of the rotation angle.

3.3. Classification of Karhunen-Loeve modes. We can use the Stokes parameters for the characterization of each KL mode polarization state:

$$\begin{aligned} X &= 2\mathrm{Re}(E_+ E_-^*), \\ Y &= 2\mathrm{Im}(E_+ E_-^*), \\ Z &= (E_+ E_+^* - E_- E_-^*), \\ I &= (E_+ E_+^* + E_- E_-^*), \end{aligned} \tag{17}$$

where $E_\pm$ represent the right and left circularly polarized components of the KL mode field.

Obviously, X, Y can be expressed as polynomials in terms of coordinates x, y, thus defining a 2D vector field (2DSP) $X=X(x,y)$, $Y=Y(x,y)$. Of course, there exists the exponential factor appearing from Laguerre-Gaussian modes, but it has no influence on singular points. This 2D vector field can be associated with the autonomous dynamical system:

$$\dot{x} = X(x(t), y(t)), \quad \dot{y} = Y(x(t), y(t)), \tag{18}$$

and the classification of the KL-mode polarization pattern can be made investigating the character of the singular points (zeroes of X and Y) of this system.

There are three possibilities [49]:

• The system is gradient,

$$\partial X/\partial y = \partial Y/\partial x.$$

There exists a potential function $V(x,y)$, which should be classified using the catastrophe theory [50].

• The system is Hamiltonian. The Hamiltonian $H(x,y)$ can be introduced in such a way that

$$dx/dt = \partial H/\partial y, \quad dy/dt = -\partial H/\partial x$$

and can be classified using Birkhoff-Gustavson normal forms [52].

• General case. The singular points $X=0$, $Y=0$ should be determined and their classification can be made using the methods [53].

In the previous paper [49] we have investigated the case $F=2.5$ which corresponds to rotating transverse patterns. These regimes belonged to the gradient case. Due to the rotation of the transverse pattern and the electric field vector $Y=0$, and the KL modes are linearly polarized. The results of numerical simulation of laser dynamics are summarized in the Table 1. a, b, c, d are nonzero coefficients, $r^2=x^2+y^2$. The type of catastrophe is presented in corresponding column, where «Morse» stands for Morse-type function, «QP» and «St» denote quasi-periodic and stationary regimes, respectively.

Table 1

Catastrophe classification of 2DSP for different gain and optical power

F	gain	number KL modes	X	catastrophe	regime
1.5	0.4	1	$a+br^2-cr^4$	A_{-3}	St
1.5	0.5	1	$-ar^4$	A_{-3}	QP
1.5	0.5	2	$-ar^6$	A_{-5}	QP
1.5	0.5	3	ar^4	A_3	QP
1.5	0.5	4	$-ar^2$	Morse	QP
1.5	0.5	5	$-ar^{10}$	A_{-9}	QP
1.5	0.6	1	$a+br^2-cr^4$	A_{-3}	QP
1.5	0.6	2	$-ar^8$	A_{-9}	QP
1.5	0.6	3	ar^4	A_5	QP
1.5	0.6	4	$-ar^4$	A_{-5}	QP
2.5	0.4	1	$a-br^2+cr^4-dr^6$	A_{-7}	St
2.5	0.5	1	$a+br^2$	Morse	QP
2.5	0.5	2	$-ar^6$	A_{-7}	QP
2.5	0.5	3	ar^4	A_{-5}	QP
2.5	0.5	4	$-ar^2$	Morse	QP
2.5	0.6	1	$a+br^2$	Morse	QP
2.5	0.6	2	$-ar^6$	A_{-7}	QP
2.5	0.6	3	ar^4	A_5	QP
2.5	0.6	4	$-ar^{10}$	A_{-11}	QP
2.5	0.6	5	$-ar^8$	A_{-9}	QP
2.5	0.6	6	ar^8	A_9	QP
2.5	0.6	7	$-ar^2$	Morse	QP
2.5	0.6	8	$-ar^4$	A_{-5}	QP

Another situation was observed for $F=2.0$. In this case the transverse patterns do not rotate but oscillate, changing the orientation of the pattern, while the polarization (the azimuth and eccentricity of the polarization ellipse) of the field in a given point of the transverse plane is almost unchanged. In Fig. 10 the corresponding instant laser patterns for right and left polarization are shown.

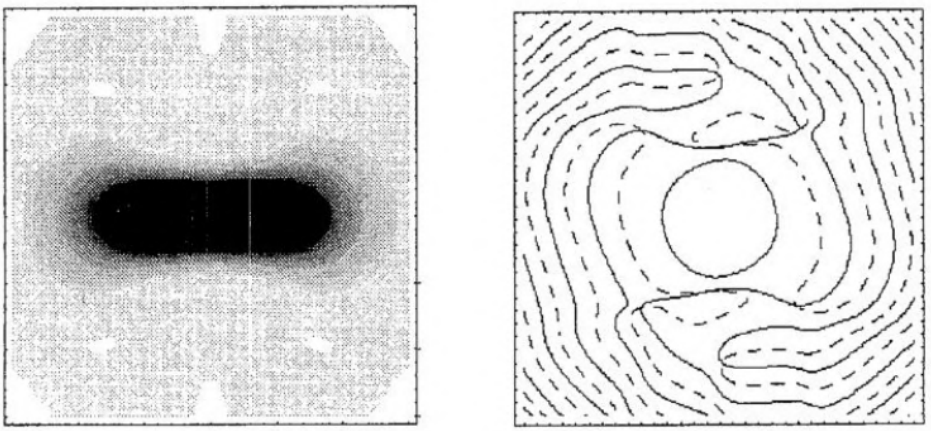

a *b*

Fig. 10. Transverse laser patterns for right-hand circular component of the electric field vector. Transverse intensity distribution $|E_+|^2$ (*a*). The curves $\mathrm{Re}(E_+)=0$ are solid and $\mathrm{Im}(E_+)=0$ are dashed (*b*)

There exist two KL modes at $F=2$, $g=0.7$ (Fig. 11).

In this case both X and Y parts of the 2D vector field of Stokes parameters are nonzero. Explicit expressions for X, Y can be written as:

$$\dot{x} = \Sigma_{i=0}^{6}\Sigma_{j=0}^{6} a_{ij}\, x^{2i}\, y^{2j}, \qquad (19)$$

$$\dot{y} = \Sigma_{i=0}^{6}\Sigma_{j=0}^{6} b_{ij}\, x^{2i}\, y^{2j}.$$

For the classification of these regimes we can use the procedure [53], which includes some steps explained below. First we should find the so-called *carrier* of the system Eq.(19). We should multiply the first equation by y and the second equation by x.

The resulting monomials $x^n\, y^m$ can be labeled by its powers (n,m), representing the corresponding point in the plane of variables (n,m). The set of all these points is the *carrier* of the system. The set of coefficients of a given monomial appearing in the right-hand part of the system is called *vector coefficients*. The points in the plane n,m form the *Newton polygon* of the system, and the part of this polygon which «looks» at the origin is *Newton diagram*.

The second step consists in simplifying the Newton diagram. The polygons can be transformed using the change of variables of the special kind (z is no more the longitudinal coordinate starting from here):

$$x = z^{p_1} w^{q_1}, \quad y = z^{p_2} w^{q_2}.$$

The matrix of indices C associated with this transformation looks as follows:

$$C = \begin{pmatrix} p_1 & q_1 \\ p_2 & q_2 \end{pmatrix}. \qquad (20)$$

In our specific case it was convenient to use C =1, 0, 1, 1. Under the transformation of coordinates the system is subjected to the corresponding transformation too:

$$\dot{zw} = \Sigma_{i=2,6}\, w^{2i}\, z\, \Sigma_{j=0,6}\, a_{i,j}\, z^{2j} \qquad (21)$$

$$z\dot{w} = \Sigma_{i=2,6}\, w^{2i}\, z\, \Sigma_{j=0,6}\, b_{i,j}\, z^{2j}$$

and, therefore, the Newton diagram can be simplified (Fig. 12).

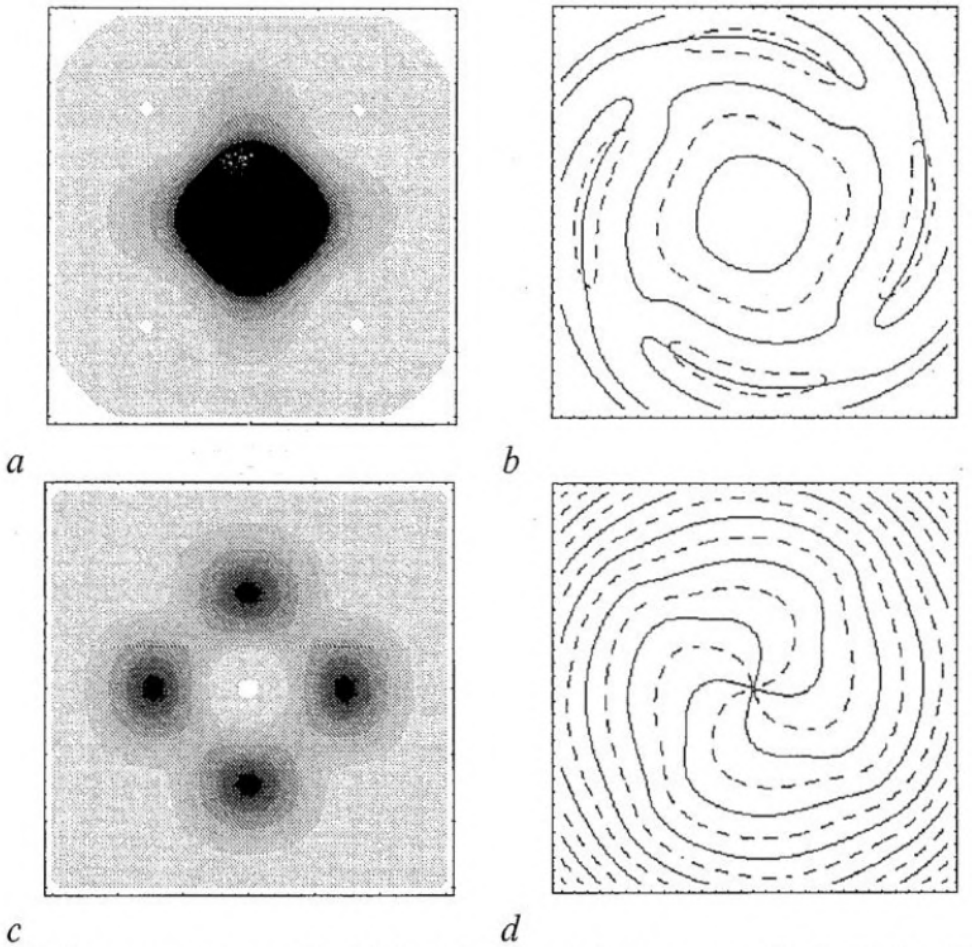

Fig. 11. The transverse patterns of the right-hand circularly polarized component of the first (*a*, *b*) and the second (*c*, *d*) Karhunen-Loeve modes. The correspondent tranverse pattern of the field is shown in Fig. 10. The eigenvalues λ_1=0.650072, λ_2=0.349926. The density (*a*, *c*) plot shows intensity of right-hand circularly polarized component of Karhunen-Loeve mode. Solid curves (*b*, *d*) shows the point of transverse plane where the real part of right-hand circularly polarized component of KL-mode is zero. Dashed curves shows the zeros of imaginary part of the same

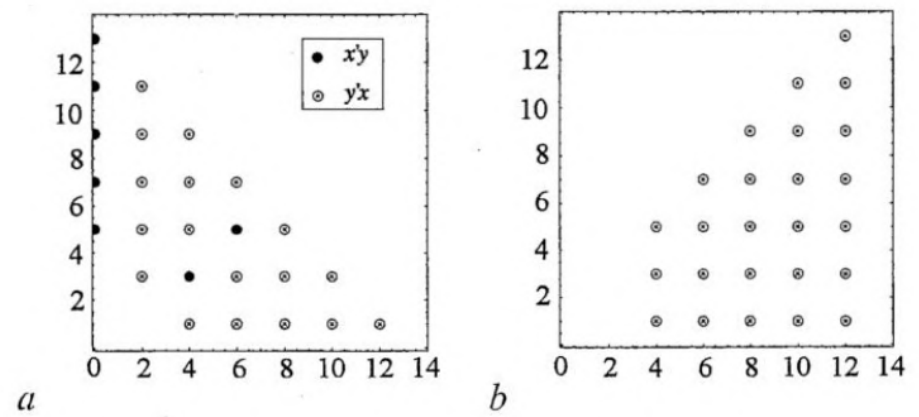

Fig. 12. Newton diagram for the right - (*a*) and the left-polarized (*b*) components of the second KL-mode after the transformation

After these transformations we can calculate the eigenvalues of the linearized system κ_1, κ_2. The signature of κ set shows the type of singularity (in our case at $z=w=0$). In this case $\kappa_1=0$,....., therefore the type of singularity is saddle-node. Using the described algorithm we can study in general the behaviour of the transverse polarization structure near the singularities of 2D vector field of Stokes parameters, which, of course, correspond to peculiarities of electric field polarization patterns. Further classification of singular points of the field is possible in the spirit of catastrophe theory for the transformed fields with linear Newton diagrams.

4. Stationary modes in boson traps

4.1. Nonground stationary states. Consider an ensemble of neutral atoms trapped in a parabolic potential. At low temperatures the Bose-Einstein condensation is possible. In the mean-field limit and s-scattering approximation the condensate is described by the collective wave function Φ that obeys the Gross-Pitaevskii (GP) equation [55]

$$i\ \partial\Phi(\mathbf{r},t)/\partial t = \hat{H}_0\Phi(\mathbf{r},t) + g|\Phi(\mathbf{r},t)|^2\Phi(\mathbf{r},t), \tag{22}$$

where g is proportional to the number of the atoms and the length of scattering,

$$\hat{H}_0 = -\,{}^1\!/_2\nabla^2 + (\omega_x{}^2x^2 + \omega_y{}^2y^2 + \omega_z{}^2z^2)/2, \tag{23}$$

x, y, z are the coordinates. The initial condition to solve Eq. (22) is

$$\Phi(\mathbf{r},t=0) = \Phi_0(\mathbf{r}). \tag{24}$$

The wave function can be normalized

$$\int_{R^3}|\Phi(\mathbf{r},t)|^2d\mathbf{r} = 1. \tag{25}$$

Let us seek the stationary solution of Eq. (22) in the form

$$\Phi^{stat}(\mathbf{r},t) = \exp(-i\,\mu t)\,\phi(\mathbf{r}). \tag{26}$$

The stationary states ϕ satisfy the stationary GP equation

$$\hat{H}_0\phi(\mathbf{r}) + g|\phi(\mathbf{r})|^2\phi(\mathbf{r}) = \mu\phi(\mathbf{r}). \tag{27}$$

For cylindrical traps $\omega_x=\omega_y=\omega_\perp$, $\omega_z<<1$. In all examples we consider $\omega_\perp=1$, $\omega_z=0$. Obviously, in this case Eq. (22) is similar to the scalar paraxial wave equation for a beam in a parabolic waveguide with Kerr nonlinearity. In contrast to optics, the nonlinear term in Eq. (22) is typically very large. Our aim here is to investigate the stationary mode with one transverse node (Fig. 13) and the possibility of a resonance transition to this state from the ground state.

For a weakly perturbed stationary state

$$\Phi^{pert}(\mathbf{r},t) = \exp(-i\,\mu t)\{\phi(\mathbf{r}) + [Cu(\mathbf{r})\exp(-i\,\omega t) + C^*v^*(\mathbf{r})\exp(i\,\omega t)]\}, \tag{28}$$

corresponding to small oscillations of the order parameter around the stationary-state value, the linearized GP equation is reduced to the simultaneous Bogoliubov equations [55]

$$\omega u = (\hat{H}_0 - \mu + 2g|\phi|^2)u + g\phi^2v; \tag{29}$$

$$-\omega v = (\hat{H}_0 - \mu + 2g|\phi|^2)v + g\phi^{*2}u, \tag{30}$$

with the orthonormalization condition

$$\int_{R^3} (u_i^* u_j - v_i^* v_j) d\mathbf{r} = \delta_{ij}. \qquad (31)$$

The oscillations (collective modes) for the one-node state considered possess some specific features in comparison with those for the ground state. One of the functions (u,v) must have no nodes, while the other has two. So we can identify the normal state by indicating the quantum numbers of the base state and of the function u. For $(u,v)_{1,2}$ (Fig. 14, *a*) the result of the numerical calculation (dotted line in Fig. 15) shows that $\omega=2\omega_\perp$ at any g. Therefore, this state is an analog of the monopole mode of the ground state. For $(u,v)_{1,0}$ (Fig. 14, *b*) the dependence of the frequency upon g is shown in Fig. 15 with dashed line. This mode, corresponding to exotic oscillations, should occur with the package radius and, therefore, the potential energy, being constant, while the kinetic energy exchanging with the energy of atomic interaction.

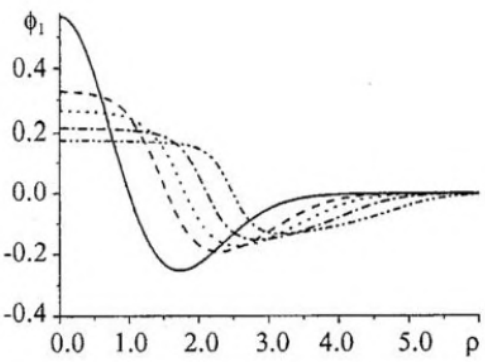

Fig. 13. One-node stationary wave function versus the distance from the trap axis. g=0 (solid line), g=50 (dashed line), g=100 (dot line), g=200 (dash dot), g=400 (dash dot dot)

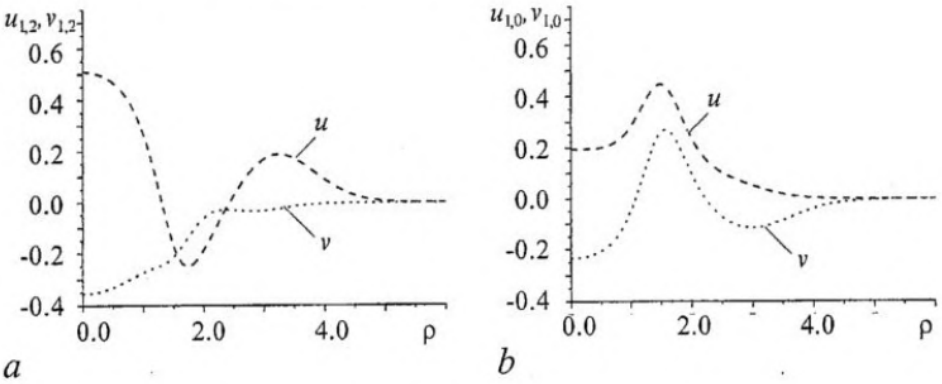

Fig. 14. Collective modes for one-node stationary state,g=50

Fig. 15. Characteristic frequencies: the difference between the potentials corresponding to one-node stationary state and the ground state (solid line); the kinetic-interaction exchanging frequency (dashed line); the averaged square radius oscillation frequency(dotted line)

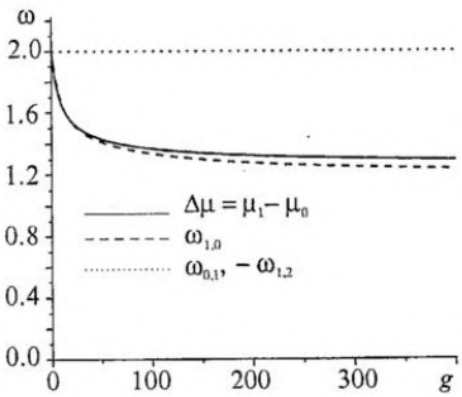

4.2. Excitation of the non-ground states. Consider a harmonic external perturbation that may be caused, e.g., by the variation of the trap parameters. In this case the GP equation may be written in the form

$$i\,(\partial\Phi(\mathbf{r},t)/\partial t) = [\hat{H}_0 + g|\Phi(\mathbf{r},t)|^2 + \kappa\sin\Omega t\,(x^2+y^2)]\Phi(\mathbf{r},t). \qquad (32)$$

Let us take the ground state as the initial one

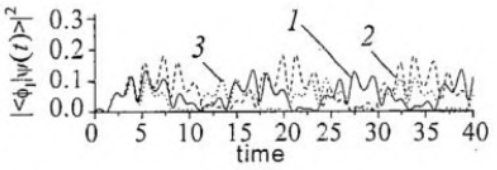

Fig. 16. Dynamics of the projection of the ground state to the one-node state under the harmonic excitation: «on-resonance» frequency (*1*, $\Omega=\Delta\mu=$ $=1.43017$), positive detuning (*2*, $\Omega=\Delta\mu+0.1$), negative detuning (*3*, $\Omega=\Delta\mu-0.1$). The maximal value is achieved for the positive detuning, because the corresponding Ω is the closest to the collective mode frequency $\omega_{0,1}=2$, $g=50$, $\kappa=0.1$

$$\Phi(\mathbf{r},t=0) = \phi_0(\mathbf{r}). \qquad (33)$$

Earlier it was supposed [56] that the transitions between the stationary states are possible under the action of a resonance external field. It is well known that for linear oscillator the maximal rate of a transition to a fixed state is limited because the energy spectrum is equidistant. Nonlinear operator eigenvalue problem (27) yields a non-equidistant spectrum. This fact was noted in [56] as the case for the applicability of the two-level approximation and possibility of creating the non-ground state. However, the results of our direct numerical solution (32, 33) contradict to this hypothesis. We found that, firstly, there is no resonance at $\Omega=\Delta\mu=\mu_i-\mu_0$ for any i and any g, and, secondly, the population of the non-ground state is oscillating from 0 to some maximal value, which increases with the growth of κ, but tends to the saturated value <40%, that accords with the maximal transition rate for a simple linear oscillator (see Fig. 16). We observed only resonances associated with the collective modes, i.e., at $\Omega=\omega$, see Eqs .(29, 30). This result is easy to explain. While the wave function of the system is close to a certain stationary state, another stationary states does not exist, because of the different effective potential in Eq.(27). The result of [56] can be a consequence of using one-parametric variational functions for the solution of Eq.(27). As a result, the authors of [56] found that $\Delta\mu\to\infty$ when $g\to\infty$, so, the averaging technique and the two-level approximation hold when g is big enough. Actually, as seen in Fig. 15, $\Delta\mu$ tends to a constant for big g.

Conclusions

Using the numerical simulations within the framework of full spatio-temporal model, we have analysed the pulse train characteristics of the Kerr-lens mode-locked laser. At the threshold the pulses have the hyperbolic secant shape. We have found that the gain depletion due to the finite relaxation time of the medium response leads to the asymmetry in the beam size variation. The gain increase leads to the distortion of the hyperbolic secant pulse shape and to deep beam size variation during the pulse. The effect of finite-time relaxation and gain saturation leads to the nonlinearity in the calculated beam transmittance at the output aperture.

In the absence of the third-order dispersion the pulse remains symmetric, but the beam size demonstrates pronounced asymmetry.

We have found that in the mode-locked regime only single solitonic solutions are stable. The gain increase leads to instabilities of pulse train. The threshold of the non-periodical oscillations of the beam shape is decreased with the decrease of the GVD and with the increase of the amplitude modulation coefficient. In quasi-periodical regimes the output power spectrum depends on the GVD coefficient and the frequency spacing between the transverse modes of the empty cavity. The coupling of multiple transverse modes leads to the sweeping of the beam size. This result is in agreement with experimental investigations.

The presented model makes it possible to obtain the full information about the spatio-temporal evolution of the pulse train. The temporal and transverse beam reshaping becomes important for femtosecond pulses. Our approach to the description of pulsed

beams can be applied in modeling femtosecond laser dynamics without the approximation of slowly varying amplitude.

We present the algorithm for the classification of different dynamics of transverse polarization patterns based on the calculation of eigenmodes (Karhunen-Loeve modes) and eigenvalues of the two-point correlation matrix, expressed via the time average of the products of the electric field components. The use of the vector Karhunen-Loeve modes allows one to select the group of transverse modes which determine the laser dynamics. These KL modes form the orthogonal basis and provide the optimal description of the dynamics of the vector field laser. Using numerical simulation of the polarization transverse pattern dynamics in a Zeeman laser, it was demonstrated that the number of essential KL modes is not so large (four in the regimes considered), while the number of Laguerre-Gaussian modes necessary to reproduce the laser dynamics is several hundreds. The regimes corresponding to the rotation of the pattern with nearly constant angular velocity were investigated as well as the regimes with oscillating patterns and nearly constant polarization parameters.

For the classification of vector transverse patterns we propose to investigate the behaviour of the polynomials representing the KL modes or the total field in the vicinity of its singular points in the transverse plane, namely, to investigate the 2D vector field of the Stokes parameters X, Y.

Non-ground stationary states of Bose-Einstein condensate of trapped atoms were studied numerically solving the strongly nonlinear Gross-Pitaevskii equation for the collective wave function. Small harmonic perturbations of these states described by Bogoliubov equations revealed essential difference between the ground stationary state and the ones having one transverse node. In contrast to earlier assumptions, we have demonstrated that in the strongly nonlinear system under consideration the periodic perturbations are unable to produce resonant transitions from the ground state to one-node non-ground states.

This work was supported in part by grant REC-006 of the US Civilian Research and Development Foundation for the Independent States of the Former Soviet Union (CRDF).

References

1. *Krausz F., Fermann M.E., Brabec T., Curley P.F., Hofer M., Ober M.H., Spielman C., Winter E. and Schmidt A.J.* // IEEE J. of Quantum Electron. 1992. Vol. 28. P. 2097.

2. *Akhmanov S.A., Vysloukh V.A., Chirkin A.S.* Optics of femtosecond laser pulses, Springer, New Yourk, 1992.

3. *Brabec T. , Spielmann C. , Krausz F.* // Opt. Lett. V. 16. P. 1961 (1991).

4. *Haus H.A., Fujimoto J.G., Ippen E.P.* // J.Opt. Soc.Am. B, Vol.8, № 10, P.2069 (1991).

5. *Magni V. , Cerullo G. , De Silvesrtri S.* // Opt. Commun. 101, P. 365, 1993.

6. *Cerullo G., De Silvesrtri S. and Magni V.* // Opt. Letters. 19, № 14, pp.1040-1042, 1994.

7. *Krausz F., Brabec T., Spielman Ch.* // Opt. Lett. Vol. 16., № 4. P. 235 (1991).

8. *Haus H.A., Fujimoto J.G., Ippen E.P.* // IEEE J. of Quantum Electron. 28, pp. 2086-2096, 1992.

9. *Bouma B.E., Ramaswamy-Paye M., Fujimoto J.G.* // Appl. Phys. B. Vol. 65, P. 213-220 (1997).

10. *Barbosa E.A., Vierra N. D.*// Optics Commun. V. 188. P. 205-211 (2001).

11. *Bohn M.J., Jones R.J., Diels J.-C.* // Optics Communications, V. 170, P.85-92, (1999).

12. *Cerullo G., De Silvesrtri S., Magni, Pallaro L.* // Opt. Letters. 19, № 11, pp. 807-809, 1994.

13. Alfrey A.J. // IEEE J. of Quantum Electron. 35, pp. 760-766, 1989.

14. Hermann J. // J.Opt.Soc.Am.B, Vol. 11, № 3, P. 498-512, (1994).

15. *Garduno-Mejia J., Mohebi M., Jamasbi N*// Opt. Comm. Vol. 171. P.263-269, (1999).

16. *KalashnikovV.L., Sorokin E., Sorokina I.T.* // e-print arXiv: physics/0101004 V. 2, Jul. 2001.

17. *Kalashnikov V., Sorokin E., Sorokina I.T.* // J. Opt. Soc. Am. B. Vol. 18 (2001), № 11, P. 1732.

18. *Kalashnikov V.L.* // Optics Communications, Vol. 192, P. 323-331 (2001).

19. *Haus H.A., Sorokina I., Sorokin E.* // J. Opt. Soc. Am. B. Vol. 15 (1998). P.223.

20. *Kutz J.N., Collings B.C., Bergman K. and Knox W.H.* // IEEE Journal of Quant. Electron., Vol . 34, № 9. P. 1749-1757, (1998).

21. *Xing Q., Chai L., Zhang W. and Wang C.* // Opt.Comm. V. 162, P. 71, (1999).

22. *Kovalsky M.G., Hnilo A.A., Gonzlez Inchauspe C.M.F.* // Opt. Lett. Vol. 24, 22. P.1638-1640 (1999).

23. *Cote D., van Dier H.M.* // Opt. Lett V.23, N.9, P.715-717, (1998).

24. *Bolton S.R., Jenks R.A., Elknton C.N., Sucha G.* // J.Opt.Soc.Am. B. Vol. 16. P.339, (1999).

25. *Spence D.E., Kean P.N., Sibbet W.* // Opt. Lett. Vol. 16. P.42 (1991).

26. *Kalashnikov V.L., Poloyko I.G., Mikhailov V.P., von der Linde D.* // J.Opt.Soc.Am B. Vol. 14, N.10, (1997).

27. *Ming-Dar Wei, Wen-Feng Hsieh* // Opt. Comm. Vol. 168, P. 161-166, (1999).

28. *Melnikov L. A., Veshneva I.V., Konukhov A.I.* // Chaos, Solitons & Fractals 4, pp. 1535-1546, 1994.

29. *Nakazawa M., Kubota H., Tamura K.* // IEEE J. Quant. Electron. V.34, № 7, P.1075-1081, (1998).

30. *Bolton S.R., Acton M.R.* // Phys. Rev. A. V.62., 063803, (2000).

31. *Konstenbauder A.G.* // IEEE J. Quant. Electron. V.26, P.1148, (1990).

32. *Dijaili S., Dienes A., Smith J.S.* // IEEE J. Quant. Electron. V.26, P.1158, (1990).

33. *Sanchez L.M., Hnilo A.A.* // Opt. Comm. V.199, P.189-199, (2001).

34. *Borisevich N.A., Buganov O.V, Tikhomirov S.A., Tolstorozhev G.B., Shkred G.L.* // Quantum Electronics. V.29, N.9, P.780-786, (1999).

35. *Brambilla M., Lugiato L.A., Penna V., Prati F., Tamm C., Weiss C.O.* 1991 Phys. Rev. A 43. 5090.

36. *Martin-Regalado J., Prati F., San Miguel M., Abraham N.B.*// 1997 IEEE J. of Quantum Electron. 33, 765.

37. *Abraham N.B., Arimondo E., San Miguel* // M. 1995. Opt. Comm. 117. 344.

38. *Serrat C., Abraham N.B., San Miguel M., Vilaseca R., Martin-Regalado J.* // 1996. Phys. Rev. A. 53. R3731.

39. *Freund I.* Optics Coomunications. 159. 99.

40. *Freund I.* 1999. Optics Communications. 163. 230.

41. *Lugiato L.A., Oppo G.L., Pernigo M.A., Tredicci J.R., Narducci L. M. and Bandy D. K.* // 1988 Optics Communications. 68. 63.

42. *Green C., Mindlin G.B., D'Angelo E.J., Solari H.G. and Tredicce J.R.* // 1990. Phis.Rev.Lett. 65. 3124.

43. *Stanley W.D.* // Digital Signal Processing. 1975. Reston Publishing Company, Inc.

44. *Reed I.S., Lan L.S.* 1994. // Journal of Visual Communication and Image Representation. 5. 304.

45. *Carevic D., Caelli T.* // 1997. Graphical Models and Image Processing. 59. 27.

46. *Wolf S.G., Ginosar R., Zeevi Y.Y.* // 1998. Journal of Visual Communication and Image Representation. 9. 25.

47. *Alessandro G., Oppo G.L.* // 1992. Optics Communications. 88. 130.

48. *Konukhov A.I., Ryabinina M.V., Veshneva I.V., Melnikov L.A.* // 1999. Proc. SPIE. 3726. 237.

49. *Konukhov A.I., Ryabinina M.V., Veshneva I.V., Melnikov L.A.* // 2001. Journal of Optics B: Quantum & Semicl. Optics. 3. S209-S214.

50. *Gilmore R.* Catastrophe theory for scientists and engineers. 1981. A Wiley-Interscience Publication John Wiley & Sons. 1981.

51. *Melnikov L.A., Konukhov A.I., Ryabinina M.V.* // 1998. Quantum and Semiclassical Optics. 10. 167.

52. *Moser J.K.* // Lectures on Hamiltonian systems. 1968. Mem. Amer. Math. Soc.

53. *Bruno A.D.* // 1979 M.: Nauka. 256 p.

54. *Parkins A.S. and Walls D.F.* The physics of trapped dilute-gas Bose-Einstein condensates // Phys. Reports, 303, pp.1-80,1998.

55. *Dalfovo F., Giorgini S., Pitaevskii L.P. and Stringari S.* Theory of Bose-Einstein condensation in trapped gases // Rev. Mod. Phys, 1, pp. 463-512, 1999.

56. *Courteille Ph.W. , Bagnato V.S. and Yukalov V.I.* Bose-Einstein condensation of trapped atomic gases // Laser Physics,{textbf 11}, pp. 659-800, 2001.

Saratov State University
Saratov Branch of the Institute of
Radio-Engineering and Electronics of RAS

Recieved 19.06.2002

УДК: 621.373.826

НЕЛИНЕЙНАЯ ДИНАМИКА ПРОСТРАНСТВЕННЫХ И ВРЕМЕННЫХ СТРУКТУР В ЛАЗЕРАХ И АТОМНОЙ ОПТИКЕ: ЛАЗЕРЫ С КЕРРОВСКОЙ СИНХРОНИЗАЦИЕЙ МОД, ЗЕЕМАНОВСКИЙ ЛАЗЕР, АТОМНЫЙ КОНДЕНСАТ БОЗЕ - ЭЙНШТЕЙНА

Л.А. Мельников, А.И. Конюхов, И.В. Вешнева, В.Л. Дербов, В.В. Серов

Путем математического моделирования исследованы пространственное и временное поведение лазерных и атомно-оптических систем. Рассмотрены системы в режиме возбуждения небольшого числа скалярных поперечных мод (лазер с Керровской синхронизацией мод), с неоднородным распределеним поляризации по поперечному сечению пучка в режиме возбуждения высших поперечных мод (Зеемановский лазер с большим числом Френеля и анизотропным резонатором) и возбужденные коллективные состояния конденсата Бозе - Эйнштейна нейтральных атомов, захваченных в ловушку. В работе предприняты попытки классифицировать динамику сложных поляризационных структур поля в лазере. Подходы к классификации основаны на вычислении векторных мод Карунена - Лова и описании их сингулярных точек с использованием теории катастроф, диаграмм Ньютона. Проанализировано возбуждение неосновных состояний атомного конденсата Бозе - Эйнштейна через резонансное возмущение.

Melnikov Leonid Arkad'evich was born in 1949, graduated from the Faculty of Physics of Saratov State University in 1971. Candidate of Science in Physics and Mathemathics since 1978, Doctor of Sciences in Physics and Mathematics since 1992. He is the member of the Optical Society of America and SPIE. He is head of Chair of Laser and Computer Physics of Saratov university, head of Laser and Fiber Optics Systems lab of Saratov Branch of the Institute of Radio-Engeneering and Electronics of Russian Academy of Sciences. His research and teaching interests include laser physic, laser spectroscopy, fiber optics, optical gyroscopes, nonlinear dynamics of lasers and optical systems, nonlinear propagation of lihgt beams and pulses in waveguides and resonance medium, lasers with short pulses and transverse nonlinear optics, laser diagnostics, photonic crystals and photonic crystal fibers, programming, computer physics. He is the author of more than 100 scientific papers.

Konukhov Andrey Ivanovich was born in 1972, graduated from Saratov State University in 1994. Candidate of Science in Physics and Mathemathics since 1998. He is a senior researcher of Laser and Fiber Optics Systems lab of Saratov Branch of the Institute of Radioengeneering of Russian Academy of Sciences. His research and teaching interests include nonlinear dynamics of lasers and optical systems, lasers with short pulses and transverse nonlinear optics.

Veshneva Irina Vladimirovna was born in 1966, graduated from Saratov State University in 1989. Candidate of Science in Physics and Mathemathics since 1996. Her research interests include nonlinear dynamics of lasers and optical systems. She is the grantee of 1995,1996 Soros graduate student program contest. She is a lecturer of Physic Depatment of Saratov State University.

Derbov Vladimir Leonardovich was born in 1949, graduated from the Faculty of Physics of Saratov State University in 1972. Candidate of Science in Physics and Mathematics since 1977, Doctor of Science in Physics and Mathematics since 1999. A member of SPIE. Head of Chair of Theoretical and Nuclear Physics of Saratov State University. His research and teaching interests include quantum theory of atoms and molecules in strong electromagnetic fields, laser spectroscopy, nonlinear optics, nonlinear dynamics of laser beams and pulses in resonance media, numerical modeling of nonlinear optical phenomena. He is the author of more than 120 scientific publications.

Serov Vladislav Victorovich was born in Ussuriysk (1976), graduated from Saratov State University in 1999. In the present time he is a post-graduated student of the chair of Theoretical and Nuclear Physics of the Saratov State University. He is the author of the 10 articles. Research interests and specialization: numerical modeling, atomic and laser physics.